

Active Power Control of DFIG-Based Wind Farm for Improvement of Transient Stability of Power Systems

Arghya Mitra and Dheeman Chatterjee, *Member, IEEE*

Abstract—This paper proposes a method to control the output power of a wind farm with the aim of improving the transient stability of a multi-machine power system. Doubly fed induction generators (DFIG) are considered for the variable speed wind farms. The variation of the frequency of the DFIG terminal bus is used to modulate the torque reference and thus the output power of the DFIG in the post-disturbance condition. This in turn modifies the electrical power of the nearby alternators and causes improvement of stability. The proposed control technique is validated in WSCC 3-machine 9-bus system and IEEE 16-machine 68-bus system. The study is carried out in PSCAD/EMTDC as well as in MATLAB platforms.

Index Terms—Doubly fed induction generator, field-oriented control, power system, transient stability, wind power.

I. INTRODUCTION

THE environmental impacts and diminishing reserve of fossil fuel is forcing the power system planners across the globe to look for increased use of renewable energy. Until now, wind energy is the cheapest of the commonly used renewable sources and hence its percentage share in the total power generation is increasing considerably in many countries. To begin with, fixed speed wind turbines and squirrel cage induction machines were used for wind power generation. Subsequently, doubly fed induction generator (DFIG) were introduced which uses power electronic converters in its rotor circuit to enable operation in both sub-synchronous and super synchronous speed regimes extracting maximum power from wind [1]. Permanent magnet synchronous machines can also be used for generating wind power, though this requires converters of higher capacity which makes it a costlier option.

Wind power generation is variable in nature due to variability of wind speed. Grid integration of this variable power in increasing capacity raises concern about its impact on the stability of the power system [2]–[6]. On the other hand, the possibility of the use of DFIG-based wind generation for overall system damping, voltage support and short term frequency support have also been investigated [7]. A power system stabilizer (PSS) for DFIG is proposed in [8]. A damping controller for DFIG using bacterial forging technique is introduced in [9]. Studies are carried out to improve the transient stability of the DFIG based

power system with the use of battery storage unit [10]. A decoupled control strategy has been proposed in [11], where the grid side converter (GSC) acts as STATCOM and the DFIG behaves like a fixed speed machine during disturbance, to improve the system stability. To improve the grid robustness two algorithms were proposed in [12]. The first algorithm is based on primary frequency control with filtered split controller and the other is referred to as torque speed controller which uses the pitch controller for improving the active power control of wind generator.

In this paper, a method is proposed to control the output power of a DFIG based wind farm for a short time span during the post-fault condition with the aim of improving the transient stability of the system. This is achieved by modifying the reference for the electromagnetic torque of the DFIG depending on the frequency of its terminal bus. As a result, variation of wind power takes place in such a way that it helps to restore the balance of mechanical and electrical power of the nearby alternator(s), thus causing an improvement in the transient stability of the system. The effectiveness of the proposed controller is verified for constant as well as variable wind speed conditions. The proposed method is also tested considering multiple wind turbine-generators (in a wind farm) experiencing the same wind profile at some time lag. PSCAD/EMTDC simulator is a standard tool used for electro-magnetic transient program and has been used for studying grid connected wind generator in [13]–[16]. In the present work also, the simulation is carried out in PSCAD/EMTDC as well as in MATLAB platforms. The systems used for the study are WSCC 3-machine 9-bus system and IEEE 16-machine 68-bus system.

II. MODEL OF THE WIND FARM AND POWER SYSTEM

The wind farm is formed by a number of wind turbines and generators connected in parallel. However, in this paper, the wind farm is represented by an aggregated model.

A. Modeling of the Wind Turbine and the DFIG

The wind turbine and the DFIG rotating mass is represented by the two mass model [17]–[20] as shown in the following:

$$\frac{d\omega_r}{dt} = \frac{1}{2H_g} [k_{sh}\theta_{tw} + C_{sh}\omega_{elB}(\omega_t - \omega_r) - T_e] \quad (1)$$

$$\frac{d\theta_{tw}}{dt} = \omega_{elB}(\omega_t - \omega_r) \quad (2)$$

$$\frac{d\omega_t}{dt} = \frac{1}{2H_t} [T_m - k_{sh}\theta_{tw} - C_{sh}\omega_{elB}(\omega_t - \omega_r)]. \quad (3)$$

Here ω_r and ω_t are the rotor electrical and mechanical speeds, respectively, θ_{tw} is the shaft torsional angle, H_t and H_g are the

Manuscript received February 25, 2014; revised July 19, 2014 and November 03, 2014; accepted January 20, 2015. This work was supported by the Department of Science & Technology, India, through the project number SR/S3/EECE/0043/2009. Paper no. TPWRS-00270-2014.

The authors are with the Department of Electrical Engineering, Indian Institute of Technology, Kharagpur, WB, 721302, India (e-mail: dheemanc@ee.iitkgp.ernet.in).

Digital Object Identifier 10.1109/TPWRS.2015.2397974

turbine and the generator inertia, respectively, k_{sh} and C_{sh} are the shaft stiffness and damping coefficient, respectively. T_m is the mechanical torque of the wind turbine which is a function of wind velocity (V_w) [17]–[21]. T_e is the electromagnetic torque.

Under unsaturated and balanced condition, the stator and the rotor circuits of the DFIG are represented by [17]–[19], [22]

$$\frac{di_{ds}}{dt} = \frac{\omega_{elB}}{L'_s} \times \left[- \left(R_s + \frac{(L_{ss} - L'_s)}{T_r} \right) i_{ds} + L'_s i_{qs} - \frac{e'_d}{T_r} + \omega_r e'_d + K_{mrr} V_{dr} - V_{ds} \right] \quad (4)$$

$$\frac{di_{qs}}{dt} = \frac{\omega_{elB}}{L'_s} \times \left[- \left(R_s + \frac{(L_{ss} - L'_s)}{T_r} \right) i_{qs} - L'_s i_{ds} + \frac{e'_q}{T_r} + \omega_r e'_q + K_{mrr} V_{qr} - V_{qs} \right] \quad (5)$$

$$\frac{de'_d}{dt} = \omega_{elB} \left[\omega_s \frac{(L_{ss} - L'_s)}{T_r} i_{qs} - \frac{e'_d}{T_r} + \omega_s (\omega_s - \omega_r) e'_q - \omega_s K_{mrr} V_{qr} \right] \quad (6)$$

$$\frac{de'_q}{dt} = \omega_{elB} \left[-\omega_s \frac{(L_{ss} - L'_s)}{T_r} i_{ds} - \frac{e'_q}{T_r} - \omega_s (\omega_s - \omega_r) e'_d + \omega_s K_{mrr} V_{dr} \right] \quad (7)$$

where ω_{elB} is the electrical base speed, ω_s is the synchronous speed in per unit, V_{ds} and V_{qs} are the stator d -axis and q -axis voltages, respectively, V_{dr} and V_{qr} are the rotor d -axis and q -axis voltages, respectively, i_{ds} and i_{qs} are the stator d -axis and q -axis currents, respectively, L_{ss} is stator inductance, R_s is the stator resistance, L_{rr} is rotor inductance, R_r is the rotor resistance, and $T_r = L_{rr}/R_r$. Also, e'_d and e'_q are the equivalent d -axis and q -axis source voltage behind transient impedance defined as

$$e'_d = \omega_s L_m (i_{qr} + K_{mrr} i_{qs}) \quad (8)$$

$$e'_q = -\omega_s L_m (i_{dr} + K_{mrr} i_{ds}) \quad (9)$$

where i_{dr} , and i_{qr} are the rotor d -axis and q -axis currents, respectively, $K_{mrr} = L_m/L_{rr}$, and L_m is the mutual inductance. Also

$$L'_s = L_{ss} - L_m^2/L_{rr}. \quad (10)$$

The electromagnetic torque T_e is given by

$$T_e = (e'_q i_{qs} + e'_d i_{ds}) / \omega_s. \quad (11)$$

The aggregated wind farm is connected to a load bus (bus “ m ”) of the existing power system through a double circuit line and a transformer having combined impedance ($r + jx$) as shown in Fig. 1 [23]. In Fig. 1, n_s is the gear box ratio, P_r and Q_r are rotor active and reactive power, respectively, and RSC stands for rotor side converter. The terminal of the aggregated DFIG is considered as a new bus “ n ”. Suppose, the load connected to the bus “ m ” in the original system (without

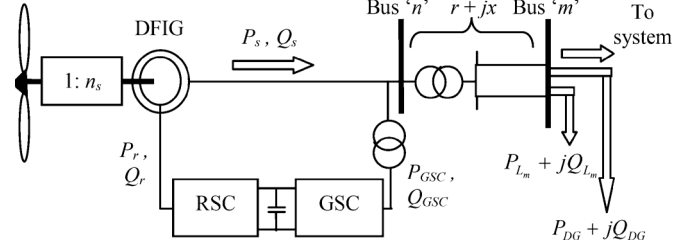


Fig. 1. Connection of DFIG to the system load bus.

wind farm) is ($P_{Lm} + jQ_{Lm}$). It is assumed that some local load ($P_{DG} + jQ_{DG}$) is present along with the wind farm. So, this local load is also considered to be connected to bus “ m ” as shown in Fig. 1 [24]. The value of this local load is considered such that under rated wind speed, the DFIG would supply this additional load as well as the losses in the connecting line and transformer. This assumption is made so that the power flow in the original network and the generation of the existing alternators remain almost unchanged (only small variations due to wind speed variability) under steady state condition. This ensures that the effects of wind power integration observed are solely due to the interaction during transient conditions.

Total active and reactive power delivered by the DFIG to the grid can be expressed as

$$P_{dg} = P_s + P_{GSC} = V_{ds} i_{ds} + V_{qs} i_{qs} + V_{dr} i_{dr} + V_{qr} i_{qr} \quad (12)$$

$$Q_{dg} = Q_s + Q_{GSC} = V_{qs} i_{ds} - V_{ds} i_{qs}. \quad (13)$$

P_s and Q_s are the stator active and reactive powers. P_{GSC} is active power flowing out of the GSC. The GSC is operated at unity power factor thus making its reactive power (Q_{GSC}) equal to zero. During fault, the rotor of the DFIG is short circuited through an external resistance (crowbar), thus making the DFIG operate as a singly excited machine. This is called the fault ride through operation [25], [26]. For a realistic simulation, the crowbar is made active after a 5-ms delay from the instant of the occurrence of the fault and is removed from the circuit after a similar time delay when the fault is cleared.

B. Modeling of Synchronous Machines and the Network

The synchronous machines are represented by the flux decay model [27], [28]. Static exciters represented by one gain and one time constant are considered along with each alternator [27]. The generator and the exciter dynamics of an m machine system is given by

$$\frac{d\delta_i}{dt} = \omega_s \Delta\omega_{r_i}, \quad i = 1, \dots, m \quad (14)$$

$$2H_i \frac{d\Delta\omega_{r_i}}{dt} = P_{m_i} - P_{e_i} - k_{D_i} \Delta\omega_{r_i}, \quad i = 1, \dots, m \quad (15)$$

$$T'_{doi} \frac{dE'_{qi}}{dt} = -\frac{x_{di}}{x_{di}} E'_{qi} + \left(\frac{x_{di}}{x_{di}} - 1 \right) V_i \cos(\delta_i - \theta_i) + E_{fd_i}, \quad i = 1, \dots, m \quad (16)$$

$$T_{A_i} \frac{dE_{fd_i}}{dt} = -E_{fd_i} + (V_{ref_i} - V_i)K_{A_i}, \quad i = 1, \dots, m \quad (17)$$

$$P_{e_i} = E'_{q_i} V_i \sin(\delta_i - \theta_i)/x'_{di} + 0.5 \left(1/x_q - 1/x'_d\right) V_i^2 \sin 2(\delta_i - \theta_i), \quad i = 1, \dots, m \quad (18)$$

where δ is the angular position of the rotor, $\Delta\omega_{ri}$ is per unit speed deviation of the rotor, H is the inertia constant, k_D is damping coefficient, P_m is mechanical power input, x_d and x_q are d -axis and q -axis synchronous reactance, x'_d is d -axis transient reactance, E'_q is the q -axis voltage behind x'_d , T'_{do} is the d -axis open circuit time constant, E_{fd} is the exciter voltage, K_A and T_A are the gain and time constant of the exciter, V is per unit terminal voltage of the machine, and θ is its angle. The transmission lines are represented by equivalent π structure. The loads are considered to be of constant impedance type.

PSCAD/EMTDC being an electromagnetic transient simulator, it includes the machine dynamics (alternator, exciter, and DFIG) as well as network dynamics. Equations (1)–(13) describing DFIG are used by PSCAD/EMTDC simulator as can be found in [22]. The flux decay model of the synchronous machine is used. The internal node of the synchronous machine is included in the network as an additional bus which is connected to the generator terminal bus through the d -axis transient reactance (x'_d) as per the standard practice [27], [28]. Hence, the dynamics due to this x'_d is also included along with the network in the PSCAD simulation. Though the fast dynamics of the network are usually neglected for transient stability studies [27], [28], here it has been included to start with because of the presence of the power electronic converters of the DFIG which are switched at higher frequencies as described in Section III. However, simulation is also carried out considering only the lower frequency (electro-mechanical) dynamics and neglecting the higher frequency dynamics using MATLAB platform and the results are compared with the PSCAD results in Section V-A.

III. MODIFICATION OF THE CONTROL STRUCTURE OF DFIG FOR STABILITY IMPROVEMENT

A. Field Oriented Control Structure of DFIG [1], [29]–[31]

The d -axis of the synchronously rotating reference frame is considered to be oriented along the stator (or bus “ n ”) voltage V_n and the q -axis is leading the d -axis. Hence

$$V_{ds} = V_n \text{ and } V_{qs} = 0. \quad (19)$$

The d -axis and q -axis components of the stator flux (ψ_s) are

$$\psi_{ds} = L_{ss}i_{ds} + L_m i_{dr} \quad (20)$$

$$\psi_{qs} = L_{ss}i_{qs} + L_m i_{qr}. \quad (21)$$

With orientation as in (19), for a sufficiently low R_s

$$\psi_{ds} \cong 0 \text{ and } \psi_{qs} \cong \psi_s. \quad (22)$$

Rearranging (11) and using (20)–(22), the electromagnetic torque can be expressed as a function of d -axis rotor current

$$T_e = - \left(\frac{L_m}{L_{ss}} \right) \psi_{qs} i_{dr}. \quad (23)$$

By rearrangement of (13) and (19)–(22), the stator reactive power can be expressed as a function of q -axis rotor current

$$Q_s = \left(\frac{L_m V_{ds}}{L_{ss}} \right) i_{qr} - V_{ds} \frac{\psi_{qs}}{L_{ss}}. \quad (24)$$

It can be seen from (23) and (24) that T_e and Q_s can be independently controlled by i_{dr} and i_{qr} , respectively. Using these relations, the field oriented control (FOC) of the DFIG rotor side converter becomes as shown in Fig. 2 [1], [29]–[31]. In Fig. 2(a), the reference torque is obtained for maximum power extraction from wind using the relation [18]

$$T_{e_{ref}} = K_{opt} \omega_r^2 \text{ if } \omega_r < \omega_{r_{rated}} \\ = T_{e_{rated}} \text{ if } \omega_r \geq \omega_{r_{rated}} \quad (25)$$

where K_{opt} in p.u. is given by

$$K_{opt} = 0.5\rho\pi R^5 C_{p_{max}} \omega_{tB}^2 / (\lambda_{opt}^3 S_B). \quad (26)$$

Here $T_{e_{rated}}$ is the rated torque and $\omega_{r_{rated}}$ is the rated DFIG speed. S_B and ω_{tB} are the base power and the base speed of the wind turbine, respectively. $C_{p_{max}}$ is the maximum value of the coefficient of performance of the wind turbine C_p when the pitch angle (β) = 0° , λ_{opt} is the tip speed ratio when $C_p = C_{p_{max}}$ [19]. The $C_p - \lambda$ curve used for this study is taken from [32]. However, the method proposed in this work has been tested with wind turbine having other $C_p - \lambda$ characteristics like that given in [18] and [19] also and the performance of the proposed model has given satisfactory result. As shown in Fig. 2(a), the reference of the d -axis rotor current ($I_{dr_{ref}}$) is compared with i_{dr} and the error signal is passed through a P-I controller to generate the rotor d -axis voltage reference ($v_{dr_{ref}}$). In Fig. 2(b), the reference for stator reactive power ($Q_{s_{ref}}$) is taken equal to the amount of reactive power to be supplied by the DFIG. The q -axis rotor current reference ($I_{qr_{ref}}$), obtained from $Q_{s_{ref}}$ by (24), is used to get the q -axis rotor voltage reference ($v_{qr_{ref}}$) through a P-I controller. The parameters of the P-I controllers of Fig. 2(a) and (b) are obtained using the pole-zero cancellation technique with the knowledge of the DFIG parameters as per the usual practice [31]. Now, d - q -0 to a - b - c transformation on $v_{dr_{ref}}$ and $v_{qr_{ref}}$ gives the rotor phase voltage references which are used as the modulating signals in PWM to generate the switching pulses for the RSC.

Similar to RSC, the stator voltage orientation is considered for the control structure of GSC also. This enables the decoupled control of active and reactive power flowing through the converter. The DC bus voltage is taken as the control variable and by maintaining this voltage constant it is ensured that the GSC allows bi-directional flow of active power between the grid and the RSC (and subsequently the rotor) via the dc bus as per the demand of the RSC. On the other hand, the reactive power flow is controlled such that the GSC is operated at unity power factor.

The pitch controller increases the wind turbine blade pitch angle to reduce the mechanical power extraction whenever the

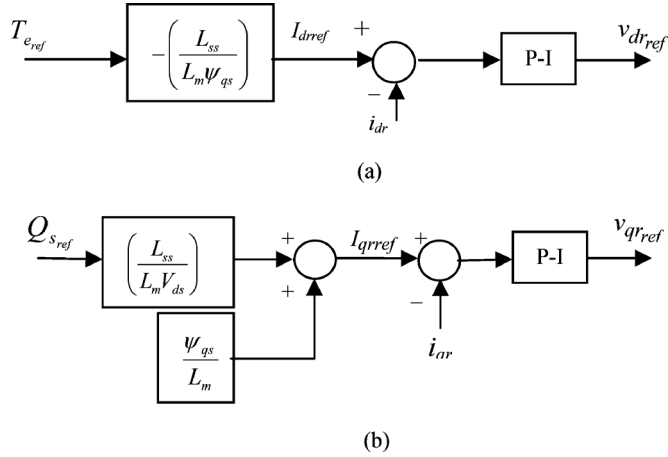


Fig. 2. (a) d -axis control block. (b) q -axis control block.

wind speed (thus ω_r) exceeds the rated value, to keep DFIG active power output $P_{dg} = P_{rated}$.

B. Modification of Field Oriented Control of the RSC

Following a disturbance (say a 3-phase short-circuit fault), the electrical power of the synchronous generators undergo some change (mostly due to changes in the bus voltages). However, the mechanical power has a larger time constant and does not change so quickly, thus resulting in some imbalance of the mechanical and electrical powers of each synchronous machine. So the relative rotor angle (δ) and the frequency of the synchronous machines undergo some excursion [following (14) and (15)] and may even become unbounded causing transient instability. If the power system consists of a wind farm, then the total power generation is the sum of the output of the synchronous generators and the wind farm. So a change in the output power of the wind farm is expected to cause changes in the output powers of the synchronous generators. Therefore, during a system disturbance, some changes in the output of the synchronous generators can be effected by controlling the output of the wind generators. Now, if this change/variation of the synchronous generator output takes place in such a way that the imbalance of its mechanical and electrical powers (caused by the disturbance) gets reduced then this will cause improvement in the transient stability. Off course the effect of this change will be more prominent if 1) the penetration of the wind farm is high and 2) the fault takes place at a location electrically not too far away from the wind farm.

With this background, a method is proposed in this paper to vary the output power of the wind generator (DFIG) during the post-fault condition in such a way that the balance of mechanical and electrical power of the nearby synchronous generators is restored, which helps to retain the synchronism. In the field oriented control of the RSC of DFIG, shown in Fig. 2, the electromagnetic torque (T_e) can be controlled by changing the torque reference T_{e_ref} without affecting the reactive power [1], [29]–[31]. Since the change of rotor speed (ω_r) is slow (due to inertia), a change of torque immediately results in a change of DFIG output power. This is achieved by introducing an additional control block (ACB), shown in Fig. 3, for modifying the torque reference, which is made active only for a short duration

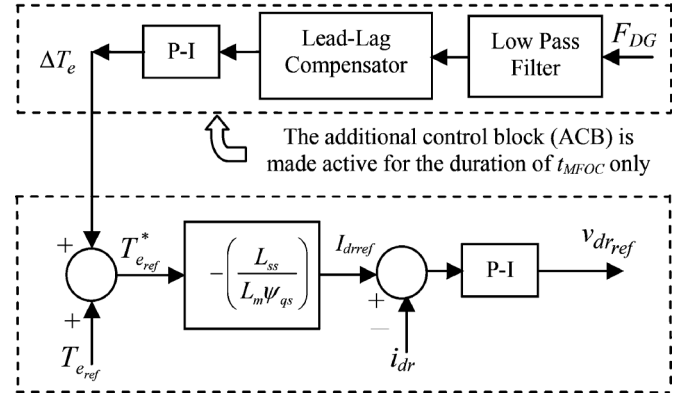


Fig. 3. The d -axis control structure for RSC with proposed modification.

just after the fault clearance. As the ultimate aim of the modification of T_{e_ref} is to oppose the imbalance of mechanical and electrical power of the nearby synchronous generators, it is required that the input variable to ACB should carry the information about that imbalance. The frequency of the DFIG terminal bus (F_{DG}) can be one such variable because the imbalance of mechanical and electrical power of the synchronous machines results in excursion of the synchronous machine rotor angle and frequency, which in turn influences the frequencies of the nearby buses (including the DFIG terminal bus). Hence, the frequency of the DFIG terminal bus (F_{DG}) is measured and used as the control signal for the ACB which is kept operative only for a short time span after the fault is cleared and the crowbar is removed.

The measured frequency, F_{DG} , contains high frequency oscillations due to network dynamics (60 Hz) which are eliminated by a low-pass filter (LPF). The corner frequency of the LPF is set at 10 Hz so that the low frequency electro-mechanical transients (0.5–2 Hz) are retained. A lead lag compensator is used to compensate the phase lag introduced by the LPF [27]. The parameters of the lead-lag compensator are calculated on the basis of the required compensation. The lead time constant and the lag time constant are taken as 1 s and 0.818 s, respectively. The filtered signal (f_{DG}) thus obtained is passed through a P-I controller and the output of the P-I controller (ΔT_e) is added to T_{e_ref} to get the modified reference torque $T_{e_ref}^*$. The proportional gain of the P-I creates damping torque and the integral part of it will influence the synchronizing torque. Excluding ACB, the remaining portion of the control structure shown in Fig. 3 is same as the one shown in Fig. 2(a). Using $T_{e_ref}^*$ as the torque reference v_{drref} is obtained. The q -axis control structure remains unchanged as in Fig. 2(b) which provides v_{qrref} . Using d - q -0 to a - b - c transformation on v_{drref} and v_{qrref} the rotor phase voltage references are obtained, which are used as the modulating signals in PWM to generate the switching pulses for the RSC. This proposed control scheme is termed as modified field oriented control (MFOC).

To summarize the choice of the controller, it can be said that

- Disturbance like fault gives rise to imbalance in mechanical and electrical power of the synchronous generators which results in excursion of rotor angle and frequency.
- Controlled variation of wind generator output during a disturbance may effect changes in the nearby synchronous

generator output power thus reducing the imbalance and aiding transient stability.

- Wind generator (DFIG) output power can be controlled by controlling its electromagnetic torque (T_e). For this, the torque reference ($T_{e,ref}$) is to be modulated.
- For modulating the DFIG $T_{e,ref}$ such that it finally result in reduced imbalance of mechanical and electrical power of nearby synchronous generators, the control variable should carry information of the imbalance.
- The frequency of the DFIG terminal bus (F_{DG}) can be one such variable because the excursion of the synchronous machine rotor angle and frequency (arising due to the imbalance of mechanical and electrical power of the synchronous generators) influences the frequencies of the nearby buses (which include the DFIG terminal bus).
- However, F_{DG} contains high frequency oscillations due to network dynamics which are eliminated using low pass filter and the resulting phase lag is compensated using a lead-lag compensator.
- The filtered signal (f_{DG}) is passed through a P-I controller. The integrator provides the synchronizing torque which helps to improve transient stability.

It may be noted that because of the presence of the integrator (of the P-I controller) in the ACB and frequency being the input, the output of the ACB (ΔT_e) will keep on increasing or decreasing. However, here the ACB is made active only for a small duration (t_{MFOC}) in the range of 0.5 s–2 s after fault clearance and the subsequent removal of the crowbar and is made inactive after that time span. As a result, the torque reference changes during that short time span (t_{MFOC}), but the change is not too high to endanger system stability. This has been illustrated with examples in Sections IV-A and IV-B. Once the ACB is withdrawn after t_{MFOC} , $T_{e,ref}$ is maintained in accordance with (25) only without being modified by ΔT_e . On the other hand, as far as the objective of influencing the first swing stability is concerned, keeping the ACB active for 0.5 s–2 s is adequate. It is obtained from further study (results discussed in Section IV-C) that a duration of $t_{MFOC} = 0.7$ s for the ACB to remain active results in maximum improvement of stability in case of the WSCC 3-machine 9-bus system.

It is to be noted that during the application of the ACB (i.e., for the 0.7 s after the fault is cleared and crowbars are removed), the maximum power tracking does not take place as the aim is to improve the system stability condition. However before and after the operating period of ACB the maximum power point tracking algorithm has been followed.

IV. IMPROVEMENT OF TRANSIENT STABILITY IN THE 3-MACHINE 9-BUS SYSTEM

An aggregated wind farm model of capacity 100 MW (20 units of rating 5 MW each [18]) is integrated with the WSCC 3-machine, 9-bus system as shown in Fig. 4 [27]. The power base is considered to be 100 MVA. The result shown in this section is obtained in the PSCAD/EMTDC platform. The disturbance considered is a 3-phase short-circuit fault in one of the load buses which gets cleared after a time t_{cl} . The maximum value of t_{cl} for which the relative rotor angles of the alternators remain bounded (synchronism is maintained) in the post fault system is called the critical clearing time (CCT). Clearly, CCT

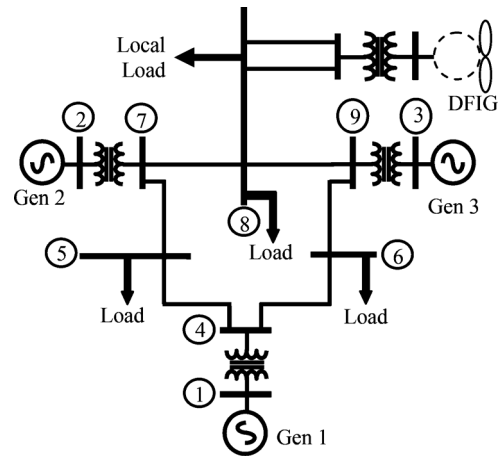


Fig. 4. WSCC 3-machine 9-bus system with DFIG connected to bus 8.

gives an indication of the transient stability margin of a power system for a given operating condition. The P-I controller parameters used in the ACB of MFOC (Fig. 3) are denoted by $(K_P)_{MFOC}$ and $(K_I)_{MFOC}$. Their values can be obtained from offline study. These values remain same for a particular wind farm location irrespective of the fault location and wind speed. In case of the 9-bus system with wind farm located at bus 8, these values are $(K_P)_{MFOC} = -1$ and $(K_I)_{MFOC} = -2500$.

A. Study With Constant Wind Speed

At first, the wind speed is considered to be constant at 13.95 m/s and the corresponding generated power is 80 MW (80% of rated power, the penetration level as defined in [24] is 20.25%). The wind farm is connected to bus 8 and a fault is considered at bus 5 at time $t = 0.5$ s. The CCT is found by carrying out repeated simulations with increased values of fault clearing time (t_{cl}). The value of CCT obtained when the RSC of the DFIG is controlled using FOC is 475 ms.

To investigate further, the variation of $T_{e,ref}$ of the DFIG with time is shown in Fig. 5(a) (by broken lines) for the case of a fault of duration $t_{cl} = 476$ ms ($>$ CCT of 475 ms) when FOC is used. Now the simulation is repeated considering the same t_{cl} ($= 476$ ms) but with the RSC being controlled by MFOC. The corresponding plot of $T_{e,ref}$ is also shown in Fig. 5(a) by solid line. The fault is cleared at $t = (0.500 + 0.476)$ s = 0.976 s, and the crowbar gets removed at $t = (0.976 + 0.005)$ s = 0.981 s. So the ACB is kept active for the duration of 0.981 s to 1.681 s (Since $t_{MFOC} = 0.7$ s).

It can be seen from the figure that during this period $T_{e,ref}$ gets reduced due the effect of ACB. The variation of the d -axis rotor voltage reference ($v_{dr,ref}$) is shown in Fig. 5(b) for both FOC and MFOC. Similarly, the variation of the electromagnetic torque (T_e) and active power output (P_{dg}) of the DFIG for both the controls, FOC and MFOC, are shown in Fig. 5(c) and (d), respectively. It can be observed that in case of control using MFOC, T_e gets reduced following the reduction of $T_{e,ref}$ during the period when the ACB is active. As a result, P_{dg} also gets reduced during this period. This reduction in P_{dg} causes an increase in the power output (P_e) of the nearby synchronous generators. The mechanical power of the synchronous generators (P_m) having a larger time constant remains almost constant and

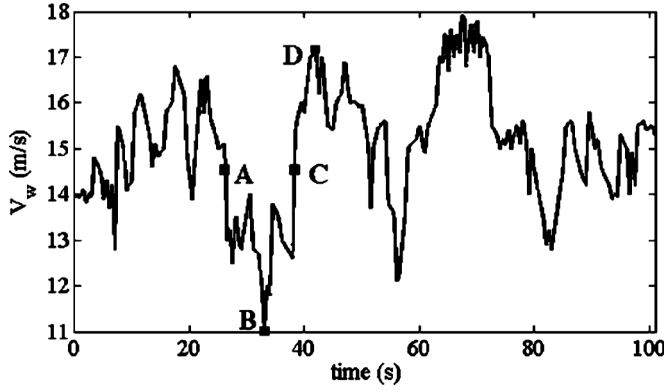


Fig. 8. Wind profile.

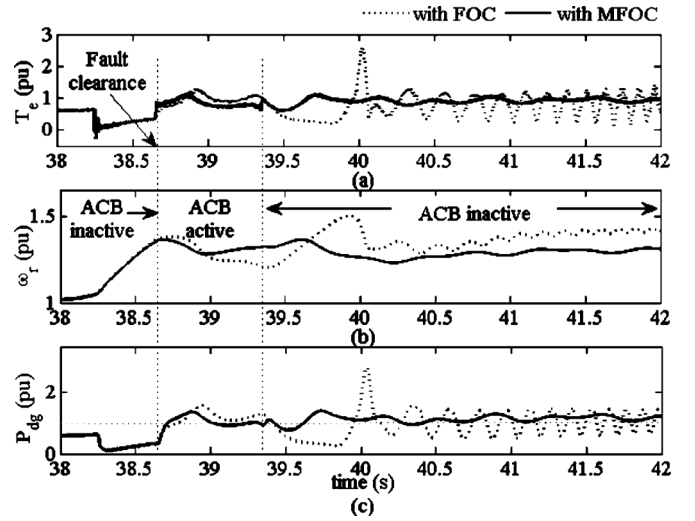
 TABLE II
 COMPARISON OF CCT FOR FOC AND MFOC (VARIABLE V_w)

DFIG & fault location	Fault instants	Wind Velocity (m/s)	Penetration level (%)	CCT (ms)		Improvement in CCT by MFOC
				MFOC	FOC	
DFIG at bus 8, fault at bus 5	A	$V_{wA} = 14.5$	22.22	155	112	43 ms
	B	$V_{wB} = 11.0$	11.25	338	309	29 ms
	C	$V_{wC} = 14.5$	22.22	442	400	42 ms
	D	$V_{wD} = 17.1$	24.10	314	283	31 ms
DFIG at bus 8, fault at bus 6	A	$V_{wA} = 14.5$	22.22	160	123	37 ms
	B	$V_{wB} = 11.0$	11.25	342	305	37 ms
	C	$V_{wC} = 14.5$	22.22	484	418	66 ms
	D	$V_{wD} = 17.1$	24.10	321	285	36 ms

profile) with slope of the plot being positive whereas at point D, the wind speed (V_{wD}) is having maximum value (with respect to the other three speeds) with slope of the plot being negative. The wind speeds at points A and C (V_{wA} and V_{wC} , respectively) are equal but the wind speed has a negative slope at point “A”, whereas it has an upward slope at point “C”. Hence, fault taking place at time instants corresponding to each of these points actually give rise to different operating conditions even when the wind farm and the fault locations are the same. At point B, the DFIG operates in sub-synchronous region whereas at the other three points it operates in super-synchronous region.

To establish this further, the CCT is computed (and shown in Table II) for all the above-mentioned cases when the RSC of the DFIG is controlled using FOC. It can be seen from the table that for a fault in any particular bus, the CCT values for the four instants of fault occurrence (“A”, “B”, “C”, and “D”) are totally different. So, during this study, all these four points are considered (one at a time) as the instant of fault occurrence to validate the generality of the observations. Now the modified controller (MFOC) is used and the CCT values are computed and shown in Table II for all the above-mentioned cases. It can be seen from the table, that in all the cases, there is an improvement in the CCT when MFOC is used. For example, when the DFIG is in bus 8 and the fault takes place in bus 5 at instant “A”, the CCT with FOC is 112 ms whereas the CCT with MFOC is 155 ms, giving an improvement of 43 ms. Similarly, when the fault takes place at bus 6 at instant “C”, there is an improvement of CCT by 66 ms when MFOC is applied.

To verify the result, the case with a fault at bus 5 at instant “C” ($V_{wC} = 14.5$ m/s) with $t_{cl} = 401$ ms is considered. The


 Fig. 9. Variation of different DFIG variables—(a) electromagnetic torque (T_e), (b) active power output (P_{dg}), and (c) electrical speed (ω_r) for the case of fault at bus 5 at instant ‘C’ in the wind profile and DFIG at bus 8.

variation of the electromagnetic torque (T_e) of DFIG under this condition is shown in Fig. 9(a) for both the controls of the RSC of DFIG, i.e., FOC and MFOC. The FOC cases are shown with dotted lines and MFOC cases are with solid line. It can be observed that the application of MFOC results in a decreased T_e as compared to the case when FOC is used. As explained before, this is caused by the action of the ACB (in case of MFOC). The variation of the rotor speed (ω_r) and active power output (P_{dg}) of the DFIG for the two cases—control using FOC (dotted line) and MFOC (solid line) are shown in Fig. 9(b) and (c), respectively. With the reduction of T_e due to the application of ACB, ω_r starts increasing. However, the change of ω_r is slow and the ACB is active only for a short time. Hence the increase of ω_r does not reach any alarming level. It can be seen from Fig. 9(c) that P_{dg} becomes less in case of MFOC during the operation of ACB. As a result of this reduction of P_{dg} , the power output of the nearby synchronous generators become higher (during active ACB) as compared to the case of control using FOC. This can be observed from the plots of variation of the output power of synchronous generator 3 (P_{e3}) shown in Fig. 10(a). This increase in P_{e3} in case of MFOC [continuous line in Fig. 10(a)] reduces the difference in the mechanical and electrical power of the synchronous generator 3 and thus improves the stability of the system. The plots of relative rotor angle δ_{31} for the same condition are shown in Fig. 10(b) for both FOC and MFOC. From the figure it is observed that δ_{31} becomes unbounded indicating instability when the RSC of the DFIG is controlled by FOC whereas δ_{31} is bounded (system stable) when MFOC is applied. The action of the ACB of MFOC stops δ_{31} from being unbounded and improves stability. This is in accordance with the fact that the CCT for system with FOC is 400 ms ($< t_{cl} = 401$ ms) but the CCT for system with MFOC is 442 ms ($> t_{cl}$).

C. Effect of Change of t_{MFOC}

The variation in the duration of applying the MFOC (t_{MFOC}) has an impact on the improvement in stability of the system.

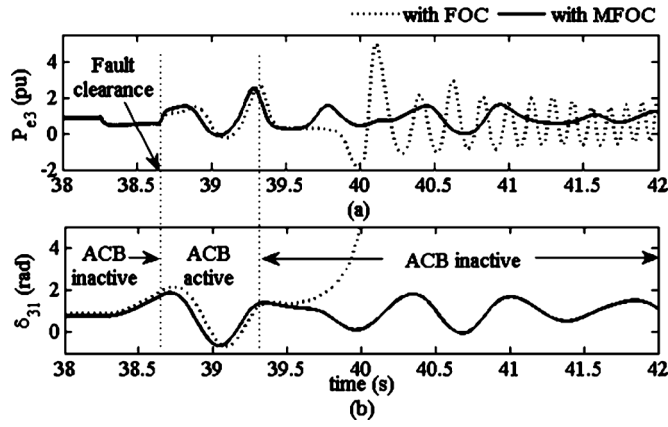


Fig. 10. Variation of synchronous generator variables—(a) active power output of generator 3 (P_{e3}) and (b) relative rotor angle (δ_{31}).

TABLE III
COMPARISON OF CCT FOR A VARYING t_{MFOC}

DFIG & fault location	CCT with FOC (ms)	Improvement in CCT by MFOC (ms)				
		$t_{MFOC} = 0.5$ s	$t_{MFOC} = 0.7$ s	$t_{MFOC} = 1.0$ s	$t_{MFOC} = 1.2$ s	$t_{MFOC} = 1.5$ s
DFIG at bus 8, fault at bus 5	112	31	43	43	43	36
	309	27	29	29	29	29
	400	33	42	40	40	40
DFIG at bus 8, fault at bus 6	283	29	31	30	30	30
	123	27	37	35	35	30
	305	28	37	28	27	27
DFIG at bus 8, fault at bus 5	418	55	66	58	58	58
	285	28	36	34	33	30

Study is done by varying the t_{MFOC} and finding the corresponding CCT for variable wind speed with an aggregated model of the wind farm. The study has been carried out for all values of t_{MFOC} between 0.5 s and 2 s at a gap of 0.05 s. However, here some of the distinct points are shown in the Table III. It can be observed from the result that the CCT improves for all the cases though the maximum improvement is obtained for $t_{MFOC} = 0.7$ s.

D. Study With a low Penetration Level

To check the effectiveness of the modified control at a lower penetration level a wind profile of the same nature as previous (Fig. 8) is considered, but with a variation in wind speed of 8–15 m/s (Fig. 11). The study is carried out considering fault at three different instants (one at a time)—“A2”, “B2”, and “C2” marked on the wind profile. The wind speed at “B2” is 8 m/s (penetration 3%) with a positive wind speed gradient. The wind speed at “A2” and “C2” are both 11.5 m/s (penetration 12.5%), though the gradient of wind speed is negative at “A2” and positive at “C2”. The DFIG operates in sub-synchronous region at all three points. The improvement in stability using MFOC (in terms of increase in CCT) is computed for the three fault instants and tabulated in Table IV.

It can be seen from the results that the application of MFOC still causes improvement in transient stability, though the range of improvement obtained is 8 ms to 15 ms, which is less as compared to the case when the penetration level is between 11.25% and 24.1%. This is because with higher penetration, there is

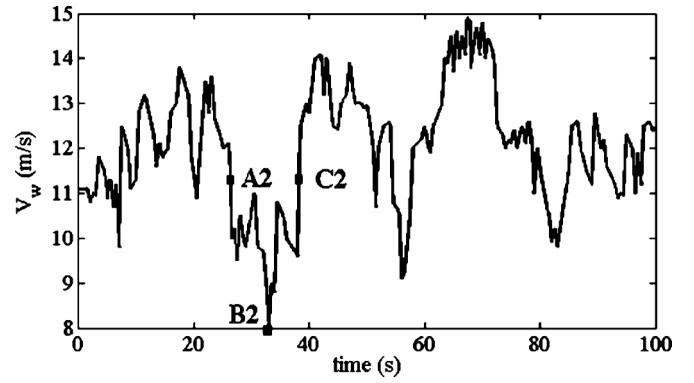


Fig. 11. Wind profile (low penetration level).

TABLE IV
COMPARISON OF IMPROVEMENT IN CCT USING MFOC FOR DIFFERENT PENETRATION LEVEL

DFIG & fault location	Fault instants	Wind speed (m/s)	Penetration level (%)	Improvement in CCT by MFOC
DFIG at bus 8, fault at bus 5	A2	11.5	12.50	10 ms
	B2	8.0	3.00	8 ms
	C2	11.5	12.50	14 ms
DFIG at bus 8, fault at bus 6	A2	11.5	12.50	15 ms
	B2	8.0	3.00	13 ms
	C2	11.5	12.50	8 ms

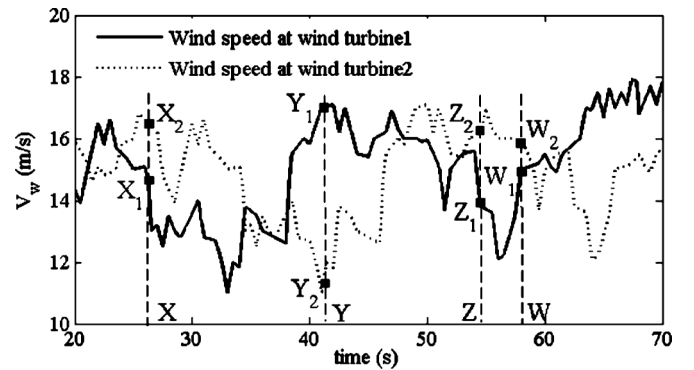


Fig. 12. Wind profiles experienced by the two wind turbines.

scope for larger change in P_{dg} (and hence P_e) by the application of MFOC.

E. Study With Variable Wind Speed (Split Wind Farm Model)

A wind farm of hundreds of MW capacity consists of a large number of wind turbines which are distributed in an area. Naturally, the wind speed experienced (and hence the mechanical torque, T_m) at a particular instant is different for each of these turbines. To include this condition in the study, the wind farm is now represented by two aggregated turbine-generator sets each having a rating half (50 MW) that of the wind farm. Also, it is considered that the two turbines are experiencing wind speed of the same profile (Fig. 8) but with a delay (of 8 s) as shown in Fig. 12. Here the profile is shown for the span from 20 s to 70 s. The delay is set on the basis of the assumption that it is the time in which the wind crosses the distance between the two aggregated wind turbines.

TABLE V
COMPARISON OF CCT FOR FOC AND MFOC (VARIABLE V_w)

DFIG & fault location	Wind Velocity (m/s)		CCT (ms)		Improvement in CCT by MFOC
			MFOC	FOC	
DFIG at bus 8, fault at bus 5	$V_{wX1}=14.5$	$V_{wX2}=16.4$	180	163	17 ms
	$V_{wY1}=17.02$	$V_{wY2}=11.4$	327	327	0 ms
	$V_{wZ1}=13.8$	$V_{wZ2}=16.2$	212	187	25 ms
	$V_{wW1}=15.0$	$V_{wW2}=16.0$	228	177	51 ms
DFIG at bus 8, fault at bus 6	$V_{wX1}=14.5$	$V_{wX2}=16.4$	184	168	16 ms
	$V_{wY1}=17.02$	$V_{wY2}=11.4$	332	332	0 ms
	$V_{wZ1}=13.8$	$V_{wZ2}=16.2$	216	205	11 ms
	$V_{wW1}=15.0$	$V_{wW2}=16.0$	230	220	10 ms

Four vertical lines marked as X, Y, Z, and W, are drawn on the wind profile to identify the four different fault occurrence instants considered here. The points of intersection of the fault instant lines with two wind profiles are X_1, X_2 for instant ‘‘X’’, Y_1, Y_2 for instant ‘‘Y’’, Z_1, Z_2 for instant ‘‘Z’’, and W_1, W_2 for instant ‘‘W’’ as shown in Fig. 12. At instant ‘‘X’’, the wind speeds experienced by the wind turbine 1 and wind turbine 2 are V_{wX1} and V_{wX2} (corresponding to points X_1 and X_2 , respectively). It can be seen that at the instant ‘‘X’’, both the profiles have negative slope. On the other hand, at instants ‘‘Y’’ both the profiles have positive slope and at instants ‘‘Z’’ and ‘‘W’’ one profile has upward slope and the other has downward slope. Study is carried out considering these four cases (one at a time) as the fault occurrence instant.

The DFIG and fault locations are considered as in Section IV-B. The P-I controller parameters $(K_P)_{MFOC}$ and $(K_I)_{MFOC}$ used in the MFOC for both the DFIGs are kept at -1 and -2500 , respectively, as in the case of aggregated wind farm model.

First the CCT is computed for the above mentioned cases with FOC and the values are shown in Table V. Then CCT is calculated for the same cases but now with MFOC and values are shown in Table V. It is seen from the table that with the introduction of MFOC in the DFIG, CCT increases for most of the cases indicating improvement in system stability. The highest improvement is found to be 51 ms for a fault at bus 5 at the instant ‘‘W’’.

It may further be observed from Table V that only in the case of fault at instant ‘‘Y’’, there is no improvement in stability. A more detailed investigation reveals that the wind speed at the instant ‘‘Y’’ on the wind profile is already very high (17.02 m/s) and has a positive slope as viewed from the further zoomed in plot of the wind profile (Fig. 13). Hence, the wind speed increases in the fault and post-fault durations resulting in an increase in ω_r . Now, the negative values of $(K_P)_{MFOC}$ and $(K_I)_{MFOC}$ in the structure of MFOC causes a decrease of P_{dg} and further increase in ω_r well above the rated speed of wind farm-1. In case of a fault of larger duration, this increase of ω_r results in instability of the DFIG itself. However, if the controller parameters are changed to positive values $(K_P)_{MFOC} = 1$ and $(K_I)_{MFOC} = 20\,000$ (only for the case of fault at instant ‘‘Y’’), an improvement in the system stability is observed (13 ms for a fault at bus 5 and 2 ms for a fault at bus 6).

However, the focus of this work is to elaborate the effectiveness of the proposed MFOC in causing improvement in transient

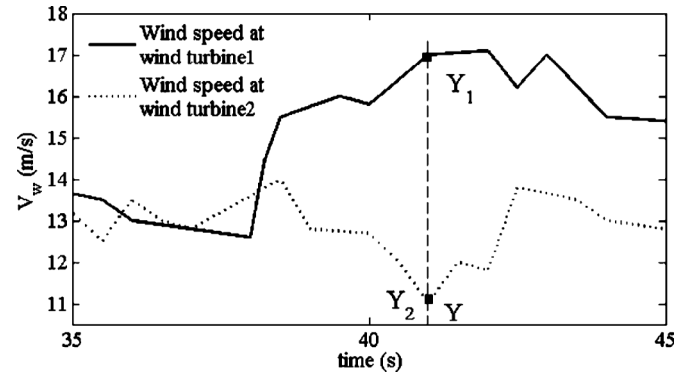


Fig. 13. Wind profile: Zoomed view of Fig. 12.

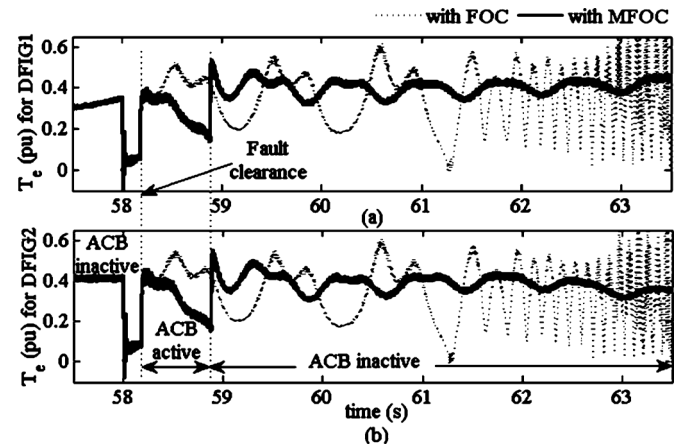


Fig. 14. Variation of electrical torque (T_e) of (a) DFIG1 and (b) DFIG2 for wind farm at bus 8 and fault at bus 5 at an instant ‘‘W’’ in the wind profile.

stability and not modifying the controller parameters adaptively for few extreme cases like the instant ‘‘Y’’ in the wind profile. It should also be noted that even for this extreme case, the stability condition does not deteriorate with the use of the negative valued controller parameters (improvement in CCT is 0 ms and not negative in Table V). On the other hand, for all other cases shown in Table V, there is considerable improvement in the transient stability condition.

To verify the result, the fault at bus 5 at an instant ‘‘W’’ is considered. The plots of T_e of the two DFIGs are shown in Fig. 14(a) and (b) for the system with FOC and with MFOC. The fault duration is taken as 178 ms, which is more than the corresponding CCT (177 ms) with FOC.

It can be seen from the figure that in case of DFIG controlled by FOC, the torque becomes oscillatory indicating instability of the system while it approaches a steady value with the application of MFOC which indicates a stable system. The modification in T_e is slightly different for the two DFIGs as the wind speeds and slopes of wind speed variation experienced by the corresponding turbines are different.

V. IMPROVEMENT OF TRANSIENT STABILITY IN IEEE 16-MACHINE 68-BUS SYSTEM

A. Reduced Model for Study in Large Systems

Until now, all the simulations were carried out in PSCAD which includes the machine dynamics (alternator, exciter and

DFIG), network dynamics and the dynamics of the converter controllers. However, for a system with large number of buses, the computational time will be very high if all these dynamics are considered. For transient stability study, it is customary to neglect the dynamics of the transmission network and the stator of the synchronous machines and represent them by algebraic equations [27], [28]. Similarly, the dynamics of stator and rotor of the DFIG can be neglected and they can be represented using the algebraic equations obtained by equating the left hand sides of (4)–(7) to zero [1], [2], [21]. The inner loop current controllers of the rotor side converter of the DFIG (the P-I controllers in Fig. 2) are fast [30] and hence can be neglected. Therefore, it is assumed that the rotor d -axis and q -axis currents are equal to $I_{d\text{rref}}$ and $I_{q\text{rref}}$, respectively. Also, the time constant (τ) for the DFIG rotor current can be expressed as [29], [30], [33], [34]

$$\tau = \frac{\sigma L_{rr}}{R_r}, \text{ where } \sigma = 1 - \left(\frac{L_m^2}{L_{ss} L_{rr}} \right). \quad (27)$$

For the DFIG considered in case of the 9-bus system, the values of $\sigma = 0.0246$, $L_{rr} = 0.0027\text{H}$, $R_r = 0.0014\Omega$. The time constant found using (27) is $\tau = 48$ ms. This is small enough as compared to the electro-mechanical transient (0.5–2 Hz) and hence it is reasonable to neglect the rotor transients.

The rotor voltage and the stator current are obtained by solving the stator and rotor algebraic equations. The dynamics of the grid side converter of the DFIG is also neglected. With these assumptions, the simulation of the system involves the solution of a set of differential and algebraic equations (DAE) which is carried out as in [27] and [28]. This study with the reduced order model (ROM) of the system is carried out in MATLAB. To verify the validity of simulation results considering all these assumptions, results obtained in the 9-bus system using the ROM are compared with those obtained earlier with full order model (FOM) using PSCAD/EMTDC. The plots of relative rotor angle δ_{21} of the alternators and DFIG electro-magnetic torque (T_e) for the FOM and the ROM are shown in Fig. 15. The plots are obtained for the case when the wind farm (represented by single aggregated wind turbine-DFIG) with FOC is connected to bus 8 and a fault of duration 400 ms takes place at bus 5 at the instant corresponding to point “C” in the wind profile of Fig. 8. It can be seen from the figure that the variation of δ_{21} in the two cases are almost identical. The variation of T_e of DFIG are also similar, though, there is some additional high frequency oscillation in case of FOM which is making the plot appear thicker. This is due to the stator and rotor dynamics and do not interfere with the electro-mechanical transient involved in transient angular stability. The plots of δ_{21} for a fault at bus 5 at an instant “B” at single aggregated wind farm with MFOC can be seen in Fig. 16. The variations are again almost similar as in the previous case. Therefore the ROM of DFIG can be used for transient stability study without much loss of accuracy.

B. Results in the 68-Bus System

The IEEE 16-machine, 68-bus system [35] is shown in Fig. 17. The power base is considered to be 100 MVA. The wind farm capacity used for this study is taken as 500 MW

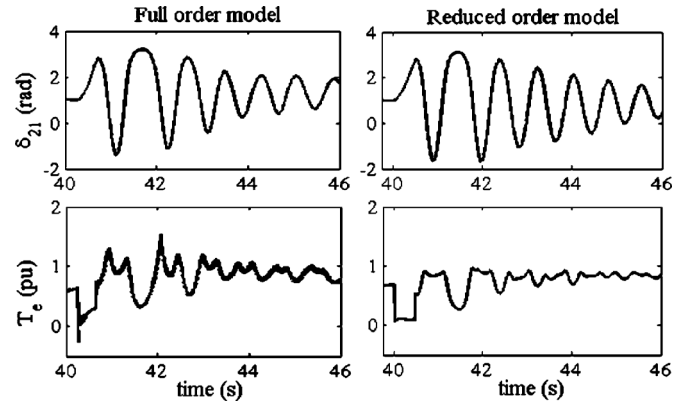


Fig. 15. Comparison of plots for full order and reduced order model with FOC for DFIG at bus 8 and fault at bus 5 at “C” in wind profile.

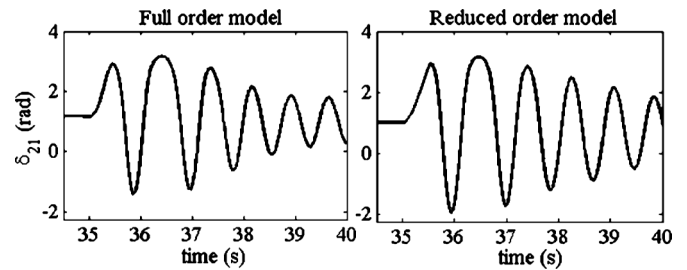


Fig. 16. Comparison of δ_{21} for full order and reduced order model with MFOC for DFIG at bus 8 and fault at bus 5 at “B” in wind profile.

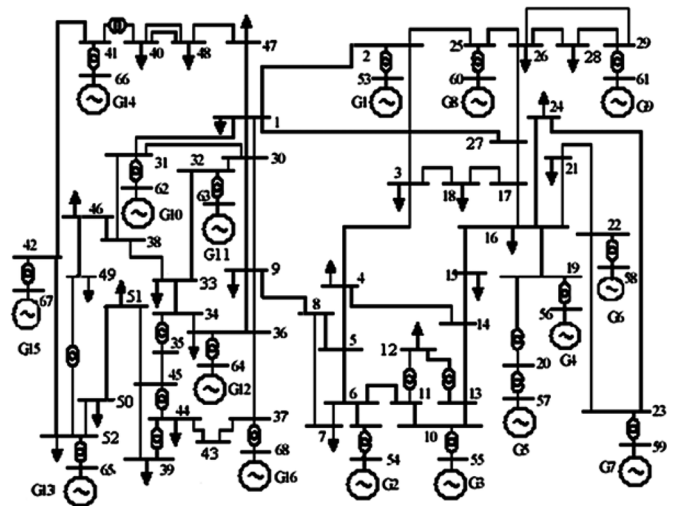


Fig. 17. IEEE 16-machine 68-bus system.

(penetration level is 2.75%). At first, the wind farm is considered to be connected at bus 28. For studying the effect of the DFIG on system stability, a three-phase short-circuit fault is considered in a group of closely located buses as shown below [36]. This group is denoted here by Gr-I.

Gr-I: 1, 2, 3, 17, 18, 25, 26, 27, 28, 29, 53, 60, 61

This choice of fault location is based on the fact that in a large power system, the effects of a disturbance at a particular location are prominent on the nearby buses. The system is simulated in MATLAB with a reduced model of DFIG. The study is carried out considering constant as well as variable wind speeds with both aggregated and split wind farm model as in Section IV.

For the case of a fault (of duration 287 ms) at bus 28, at an instant corresponding to point “B” in the wind profile of Fig. 8, plot of DFIG electromagnetic torque (T_e) is shown in Fig. 18(a) both for FOC (dotted line) and MFOC (solid line). In this case, single aggregated wind farm is considered. The CCT for control with FOC is 286 ms. It is seen from Fig. 18(a) that the MFOC reduces T_e during the active region of MFOC. The corresponding variations of DFIG speed (ω_r) and its active power output (P_{dg}) are shown in Fig. 18(b) and (c) respectively. Because of the slow change of ω_r , the reduction in P_{dg} is quite appreciable in Fig. 18(c) during the action of ACB. The variation of the relative rotor angle (δ_{9-1}) for the two cases (i.e., control using FOC and MFOC) are shown in Fig. 19. Here δ_{9-1} is the rotor angle of synchronous generator 9 (nearby bus 28) relative to the rotor angle of synchronous generator 1 (taken as the reference). It can be seen from Fig. 19 that the system loses its synchronism for the first case (control with FOC) while it retains its synchronism in case of control with MFOC. This is due to the reduction in P_{dg} which ultimately reduces the excursion of rotor angles of nearby alternators and improves the stability. The CCT with MFOC actually increases to 345 ms.

Study is continued by putting the DFIG at bus 16 and considering the fault in the group of closely located buses (Gr-II) as follows [36].

Gr-II: 15, 16, 17, 18, 19, 20, 21, 22, 23, 24, 27, 56, 57, 58, 59

The values of K_P and K_I , the P-I controller parameters in the structure of MFOC, for 68-bus system, are as shown in Table VI. These values remain same for a particular wind farm location irrespective of the fault location and wind speed as before. As in Section IV-C here also the study has been carried out for all values of t_{MFOC} between 0.5 s and 2 s at a gap of 0.05 s. Table VI indicates the values of t_{MFOC} which give maximum improvement in stability in terms of CCT for two different locations of wind farm in two different groups of buses. Some of the comparative result of CCT both with FOC and MFOC for these groups is tabulated in Table VII for variable wind speed in single aggregated wind farm only. The fault instants are considered as in Section IV.B. It can be observed from the table that there is always an improvement in stability with the introduction of MFOC. The highest improvement in CCT is found to be 67 ms with a fault at bus 28 at an instant “C” (in Group—I).

VI. CONCLUSION

A method to improve the transient stability condition of multi-machine power systems by utilizing the power injection from wind farms is discussed here. To achieve this, a modification is proposed in the controller of the rotor side converter of the DFIG. The input torque reference of the DFIG is modulated using a feedback of the frequency of its terminal bus which ultimately results in modification of the output active power of the wind farm during the post fault condition. The impact of this variation of the wind power on the excursion of the rotor angles of the nearby alternator(s) helps to improve the transient stability condition of the system. A short duration of operation of the MFOC is sufficient for the improvement in first swing stability. The impact of the modified controller is observed both for constant wind speed and variable wind speed and the study is carried out in a 3-machine 9-bus system and 16-machine 68-bus system using PSCAD/EMTDC and MATLAB.

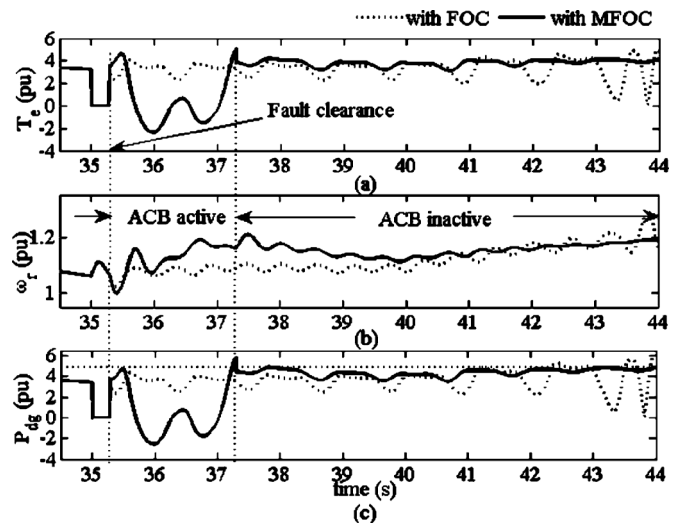


Fig. 18. Variation of different DFIG variables—(a) electrical torque (T_e), (b) rotor speed (ω_r), and (c) active power, P_{dg} for a fault at bus 28 at instant “B” in the wind profile.

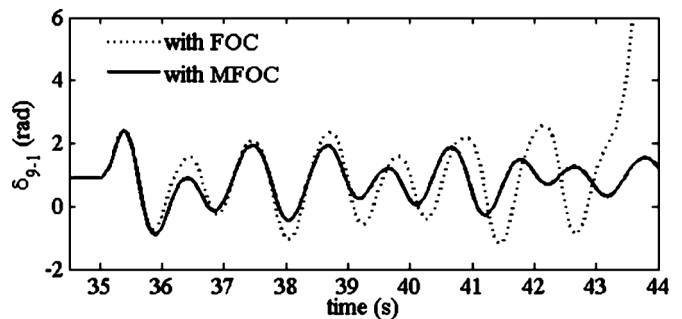


Fig. 19. Variation of synchronous generator relative rotor angle (δ_{9-1}).

TABLE VI
P-I CONTROLLER PARAMETER AND t_{MFOC} USED FOR 68-BUS SYSTEM

Group	K_P	K_I	t_{MFOC} (s)
I	10	15000	2.0
II	-10	-10000	0.7

TABLE VII
COMPARISON OF CCT FOR FOC AND MFOC (VARIABLE V_W)

Fault instants	Group	Fault at (Bus)	CCT (ms)		Improvement in CCT by MFOC
			MFOC	FOC	
A	I	28	319	284	35 ms
	II	15	325	322	3 ms
B	I	28	345	286	59 ms
	II	15	335	326	9 ms
C	I	28	338	271	67 ms
	II	15	330	325	5 ms
D	I	28	270	264	6 ms
	II	15	325	321	4 ms

ACKNOWLEDGMENT

The authors would like to thank Dr. G. Poddar of Indian Institute of Technology Kharagpur, India, for his valuable suggestions and help.

REFERENCES

- [1] M. V. A. Nunes, J. A. P. Lopes, H. H. Zurn, U. H. Bezerra, and R. G. Almeida, "Influence of the variable-speed wind generators in transient stability margin of the conventional generators integrated in electrical grids," *IEEE Trans. Energy Convers.*, vol. 19, no. 4, pp. 692–701, Dec. 2004.
- [2] N. W. Miller, J. J. Sanchez-Gasca, W. W. Price, and R. W. Delmerico, "Dynamic modeling of GE 1.5 and 3.6 MW wind turbine-generators for stability simulations," in *Proc. IEEE Power Eng. Soc. General Meeting*, Toronto, ON, Canada, Jul. 2003, pp. 1977–1983.
- [3] J. G. Sloopweg and W. L. Kling, "Impacts of distributed generation on power system transient stability," in *Proc. IEEE Power Eng. Soc. General Meeting*, Jun. 6–10, 2004, vol. 2, pp. 2150–2155.
- [4] M. J. Hossain, H. R. Pota, Md. A. Mahmd, and R. A. Ramos, "Investigation of the impacts of large-scale wind power penetration on the angle and voltage stability of power system," *IEEE Syst. J.*, vol. 6, no. 1, pp. 76–84, Mar. 2012.
- [5] D. Gautam, V. Vittal, and T. Harbour, "Impact of increased penetration of DFIG-based wind turbine generators on transient and small signal stability of power systems," *IEEE Trans. Power Syst.*, vol. 24, no. 3, pp. 1426–1434, Aug. 2009.
- [6] A. Mitra and D. Chatterjee, "A sensitivity based approach to assess the impacts of integration of variable speed wind farms on the transient stability of power systems," *Renew. Energy*, vol. 60, pp. 662–671, Dec. 2013.
- [7] F. M. Hughes, O. Anaya-Lara, N. Jenkins, and G. Strbac, "Control of DFIG-based wind generation for power network support," *IEEE Trans. Power Syst.*, vol. 20, no. 4, pp. 1958–1966, Nov. 2005.
- [8] F. M. Hughes, O. Anaya-Lara, N. Jenkins, and G. Strbac, "A power system stabilizer for DFIG-based wind generation," *IEEE Trans. Power Syst.*, vol. 21, no. 2, pp. 763–772, May 2006.
- [9] Y. Mishra, S. Mishra, M. Tripathy, N. Senroy, and Z. Y. Dong, "Improving stability of a DFIG-based wind power system with tuned damping controller," *IEEE Trans. Energy Convers.*, vol. 24, no. 3, pp. 650–660, Sep. 2009.
- [10] P. L. Seto and P. Schegner, "New control scheme for doubly-fed induction generators to improve transient stability," in *Proc. IEEE Power Eng. Soc. General Meeting*, Jun. 2007, pp. 1–10.
- [11] L. Meegahapola, D. Flynn, J. Kennedy, and T. Litter, "Active use of DFIG based wind farms for transient stability improvement during grid disturbances," in *Proc. IEEE Power & Energy Soc. General Meeting*, Jul. 2009, pp. 1–8.
- [12] E. Ela, V. Gevorgian, P. Fleming, Y. C. Zhang, M. Singh, E. Muljadi, A. Scholbrook, J. Aho, A. Buckspan, L. Pao, V. Singhvi, A. Tuohy, P. Pourbeik, D. Brooks, and N. Bhatt, Active Power Controls From Wind Power: Bridging the Gaps, NREL, Tech. Rep., Jan. 2014.
- [13] F. K. A. Lima, A. Luna, P. Rodriguez, E. H. Watanabe, and F. Blaabjerg, "Rotor voltage dynamics in the doubly fed induction generator during grid faults," *IEEE Trans. Power Electron.*, vol. 25, no. 1, pp. 118–130, Jan. 2010.
- [14] A. Luna, F. K. A. Lima, D. Santos, P. Rodriguez, E. H. Watanabe, and S. Arnaltes, "Simplified modeling of a DFIG for transient studies in wind power applications," *IEEE Trans. Ind. Electron.*, vol. 58, no. 1, pp. 9–20, Jan. 2011.
- [15] M. E. Elshiekh, D. A. Mansour, and A. M. Azmy, "Improving fault ride-through capability of DFIG-based wind turbine using superconducting fault current limiter," *IEEE Trans. Appl. Supercond.*, vol. 23, no. 3, pp. 5601204–5601204, Jun. 2013.
- [16] T. Lei, M. Ozakturk, and M. Barnes, "Modelling and analysis of DFIG wind turbine system in PSCAD/EMTDC," in *Proc. IET Int. Conf. Power Electronics, Machines and Drives (PEMD 2012)*, Mar. 2012, pp. 1–6.
- [17] F. Mei and B. Pal, "Modal analysis of grid-connected doubly fed induction generators," *IEEE Trans. Energy Convers.*, vol. 22, no. 3, pp. 728–736, Sep. 2007.
- [18] B. C. Pal and F. Mei, "Modelling adequacy of the doubly fed induction generator for small-signal stability studies in power systems," *IET Renew. Power Gener.*, vol. 2, no. 3, pp. 181–190, 2008.
- [19] F. Mei, "Small signal modeling and analysis of doubly fed induction generators in wind power applications," Ph.D. dissertation, Imperial College London, Univ. London, London, U.K., 2007.
- [20] S. K. Salman and A. L. J. Teo, "Windmill modeling consideration and factors influencing the stability of a grid-connected wind power-based embedded generator," *IEEE Trans. Power Syst.*, vol. 18, no. 2, pp. 793–802, May 2003.
- [21] J. B. Ekanayake, L. Holdsworth, and N. Jenkins, *Comparison of 5th Order and 3rd Order Machine Models for Doubly Fed Induction Generator (DFIG) Wind Turbines*. New York, NY, USA: Elsevier, 2003, pp. 207–215, EPSR 67.
- [22] M. Singh and S. Santoso, Dynamic Models for Wind Turbines and Wind Power Plants, NREL, Subcontract Rep., Oct. 2011.
- [23] P. Ledesma and J. Usaola, "Doubly fed induction generator model for transient stability analysis," *IEEE Trans. Energy Convers.*, vol. 20, no. 2, pp. 388–397, Jun. 2005.
- [24] M. K. Donnelly, J. E. Dagle, D. J. Trudnowski, and G. J. Rogers, "Impacts of the distributed utility on transmission system stability," *IEEE Trans. Power Syst.*, vol. 11, no. 2, pp. 741–746, May 1996.
- [25] A. H. Kasem, E. F. El-Saadany, H. H. El-Tamaly, and M. A. A. Wahab, "An improved fault ride-through strategy for doubly fed induction generator-based wind turbines," *IET Renew. Power Gener.*, vol. 2, no. 4, pp. 201–214, Dec. 2008.
- [26] A. D. Hansen and G. Michalke, "Fault ride-through capability of DFIG wind turbines," *Renew. Energy*, vol. 32, no. 9, pp. 1594–1610, Jul. 2007.
- [27] P. W. Sauer and M. A. Pai, *Power System Dynamics and Stability*. Hong Kong: Pearson Education Asia, 2002, First Indian Reprint.
- [28] P. Kundur, *Power System Stability and Control*. New York, NY, USA: McGraw-Hill, 1994.
- [29] R. Pena, J. C. Clare, and G. M. Asher, "Doubly fed induction generator using back-to-back PWM converters and its application to variable-speed wind-energy generation," *IEE Proc.*, vol. 143, no. 3, pt. B, pp. 231–241, May 1996.
- [30] V. Vittal and R. Ayyanar, *Grid Integration and Dynamic Impact of Wind Energy*. New York, NY, USA: Springer, 2013.
- [31] A. Yazdani and R. Iravani, *Voltage-Sourced Converters in Power Systems Modeling, Control, and Application*. Hoboken, NJ, USA: John Wiley & Sons, 2010.
- [32] P. M. Anderson and A. Bose, "Stability simulation of wind turbine systems," *IEEE Trans. Power App. Syst.*, vol. PAS-102, no. 12, pp. 3791–3795, Dec. 1983.
- [33] R. Datta, "Rotor side control of grid-connected wound rotor induction machine and its application to wind power generation," Ph.D. dissertation, Indian Inst. Sci., Bangalore, India, 2000.
- [34] J. M. Rodriguez, J. L. Fernandez, D. Beato, R. Iturbe, J. Usaola, P. Ledesma, and J. R. Wilhelm, "Incidence on power system dynamics of high penetration of fixed speed and doubly fed wind energy systems: Study of the Spanish case," *IEEE Trans. Power Syst.*, vol. 17, no. 4, pp. 1089–1095, Nov. 2002.
- [35] Power System Toolbox, Version 2.0, Cherry Tree Scientific Software.
- [36] D. Chatterjee, A. Ghosh, and M. A. Pai, "Trajectory sensitivity in distributed generation systems analysis," in *Proc. IEEE Int. Conf. Power Electronics, Drives and Energy Systems (PEDES'06)*, Dec. 2006, pp. 1–6.

Arghya Mitra received the B.E. degree in power plant engineering from Jadavpur University, Kolkata, India, in 2002 and the M.Tech. degree in electrical engineering (electrical power) from the University of Calcutta, Kolkata, India, in 2008.

He worked for six years as a Lecturer and one and a half years as Sr. Lecturer in the Department of Electrical Engineering, B. P. Poddar Institute of Management and Technology, Kolkata, India. Presently he is a research scholar in the Department of Electrical Engineering IIT Kharagpur. His research interest is power system dynamics and stability.

Dheeman Chatterjee (M'08) received the B.E. and M.E. degrees in electrical engineering from Bengal Engineering College, Shibpur, W. B., India, in 1996 and 2002, respectively and the Ph.D. degree from IIT Kanpur, U. P., India, in 2007.

He has three years of working experience in the operation and maintenance of electrical power distribution. He has been working as an Assistant Professor in the Department of Electrical Engineering, IIT Kharagpur, W. B., India, since 2008. His area of interest is integration of renewable energy and FACTS devices and their impacts on power system dynamics.